Available online at www.sciencedirect.com
ScienceDirect
Journal of Catalysis 251 (2007) 153–162
JOURNAL OF CATALYSIS
www.elsevier.com/locate/jcat

Bifunctional catalysts for single-stage water–gas shift reaction in fuel cell applications. Part 1. Effect of the support on the reaction sequence

K.G. Azzam, I.V. Babich, K. Seshan, L. Lefferts *

Catalytic Processes and Materials, Faculty of Science and Technology, IMPACT, University of Twente, P.O. Box 217, 7500AE Enschede, The Netherlands

Received 29 March 2007; revised 3 July 2007; accepted 8 July 2007

Available online 31 August 2007

Abstract

Oxide support plays a significant role in the mechanistic reaction sequence for the water–gas shift (WGS) reaction over Pt-based catalysts. In situ FTIR spectroscopic and transient kinetic studies have been used to follow the reactions that occur. CeO_2-, TiO_2-, and ZrO_2-supported Pt catalysts have been studied at 300 °C. In all cases, CO is adsorbed on Pt. The role of the support oxide is to activate water, completing the WGS reaction sequence. We have taken into consideration four different pathways that may be involved in the complex WGS reaction scheme: (A) red–ox route, (B) associative formate route, (C) associative formate route with red–ox regeneration of the oxide support, and (D) carbonate route. In the case of Pt/ZrO_2, the WGS reaction follows the associative formate route with red–ox regeneration (route C). On Pt/TiO_2, both the red–ox route (A) and the associative formate route with red–ox regeneration (C) contribute. The associative formate route (B) is the relevant reaction pathway on Pt/CeO_2.

Keywords: Water–gas shift; Platinum; Ceria; Titania; Zirconia; Reaction mechanism; Red–ox; Associative formate mechanism; Carbonate

1. Introduction

The water–gas shift (WGS) reaction is a reversible, exothermic reaction in which carbon monoxide reacts with steam to produce hydrogen and carbon dioxide:

$$CO + H_2O \leftrightarrows CO_2 + H_2, \quad \Delta H = -40.6\ \text{kJ/mol}.$$

This reaction is a crucial step in maximizing hydrogen after the conversion of hydrocarbons to synthesis gas via steam reforming or partial oxidation [1]. The demand for hydrogen is expected to increase in the future due to its use in fuel cell applications for power generation. This is because fuel cells are appreciably more efficient than current internal combustion engines and are environmentally friendly, producing no CO_x, NO_x, hydrocarbons, or soot emissions [2,3].

The state-of-the-art industrial process for WGS is carried out in two stages to overcome the thermodynamic limitation for the reaction at higher temperatures and to achieve almost complete CO conversion (unconverted CO <1000 ppm). The two steps involve a high-temperature (350–500 °C) shift (HTS) over Fe_2O_3/Cr_2O_3 catalyst, followed by a low-temperature (200–250 °C) shift (LTS) over a $Cu/ZnO/Al_2O_3$ catalyst [1]. This approach, which is currently practiced at industrial scales, is not an appropriate choice for mobile applications because of its technical complexity and the multiple stages involved [2]. A single-stage WGS conversion is thus desirable. Supported noble metal-based (e.g., Pt) catalysts are reported as promising single-stage WGS catalysts because they (i) are robust, (ii) can operate at higher temperatures where the kinetics is more favorable in contrast to Cu catalysts, (iii) are less sensitive to poisons (Cl and S) than the LTS (Cu-based) catalysts, and (iv) are more active than the HTS (Fe/Cr oxide-based) catalysts [2,3].

Recently, various catalyst compositions have been explored in WGS by varying Pt loading (from 0.1 to 5 wt%) and the oxide supports (e.g., CeO_2 [4–6], ZrO_2 [7,8], TiO_2 [9–11], $Ce_xZr_{1-x}O_2$ [12–15], $Ti_xCe_{1-x}O_2$ [16]). Activity is reported to depend on a number of factors, including catalyst prepara-

* Corresponding author. Fax: +31 53 489 4683.
E-mail address: l.lefferts@tnw.utwente.nl (L. Lefferts).

0021-9517/$ – see front matter
doi:10.1016/j.jcat.2007.07.010

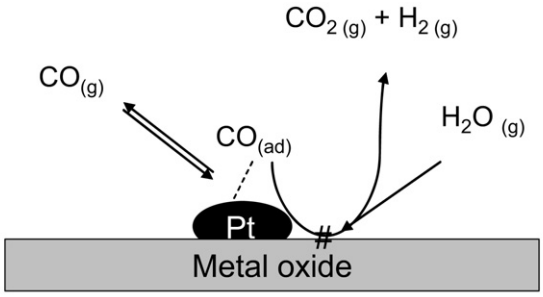

1- Formal red-ox of support with CO and H_2O [a]

$$Pt\text{-}CO + O_{(s)} \rightarrow CO_{2(g)} + *_{(s)} + Pt$$

$$*_{(s)} + H_2O \rightarrow O_{(s)} + H_{2(g)}$$

2- Formation of $CO_2 + H_2$ via OH-support and regeneration of OH by H_2O from gas phase [a]

$$Pt\text{-}CO + OH_{(s)} \rightarrow CO_{2(g)} + \tfrac{1}{2}\, H_{2(g)} + Pt + *_{(s)}$$ [b]

$$*_{(s)} + O_{(s)} + H_2O \rightarrow 2OH_{(s)}$$

[a] Due to the activation of water exclusively on the support, Pt atoms in the vicinity of the support should be involved in CO activation (20a)

[b] CO, adsorbed on Pt, is suggested to undergo WGS reaction *via* $C_xH_yO_z$ intermediate(s), for e.g., formate, [5, 6, 13, 26, 27].

Fig. 1. The role of the support in WGS reaction sequence.

tion [4,5,10,17], the nature of the support [16], testing conditions, and reactor design [18]. Despite the fact that noble metal-based catalysts are very active, their straightforward application to provide hydrogen feed for PEM fuel cells is not feasible because of limited conversion of CO due to thermodynamic constraints. This can be overcome by selective product separation to shift the equilibrium to the product side, by, for example, using a hydrogen-selective permeable membrane [19,20] or CO_2 sorbents [21]. Removal of CO by preferential oxidation or methanation are other options to further lower the CO concentration [22,23]. The experiments in this study were carried out at 300 °C, inspired by the fact that hydrogen-selective membranes are stable at those conditions.

In general, it is agreed that both the metal and the support play essential roles in the WGS reaction. Among the two reactants for WGS reaction, CO and H_2O, the latter is more difficult to activate [24] due to its thermodynamic stability. Metals such as Cu and Fe are reported to undergo oxidation by water [25], thereby activating it. However, Pt does not interact chemically with water because the PtO_x that would be formed is not thermodynamically stable [26] at WGS temperatures. Thus, for Pt-based WGS catalysts, a hydrophilic oxide support is essential to adsorb and activate water [24–30]. Therefore, such catalysts are bifunctional, with platinum activating CO and the support activating H_2O.

Different WGS reaction pathways have been suggested in the literature [4,27]; these are schematically presented in Fig. 1. Water either reoxidizes the support oxide after reduction by CO, activated on Pt, or forms hydroxyl groups and completes the catalytic cycle. The exact nature of the relevant intermediates formed and the mechanistic route(s) for the WGS reaction are still a matter of debate, however. In the case of Pt/CeO_2, the most widely studied catalytic system for WGS, two reaction mechanisms have been proposed: (i) associative (surface formate) [5,6,13,31,32] and (ii) regenerative red–ox mechanism [26,28,33,34].

In the associative mechanism [5,6,13,31,32], hydroxyl groups on the support react with CO and form surface formates. The decomposition of formate species is suggested to be facilitated by the presence of water in the gas phase and is rate-determining. During this step, hydroxyl groups are regenerated on the oxide surface. No oxygen is removed from the surface during the catalytic cycle, and the oxide does not undergo any red–ox changes during the WGS sequence. This mechanism was supported by FTIR measurements, isotope-exchange experiments, pulse-type experiments and kinetic studies of CO_2 hydrogenation (reverse WGS) [5,6,13,31,32,35]. The role of Pt is not clear from these studies and cannot be elucidated from the reaction schemes proposed. However, it has been suggested, without clear experimental evidence, that Pt aids in the generation of bridging OH groups, which are claimed to be necessary for the formation of surface formate groups. Platinum also facilitates decomposition of formate groups in the presence of H_2O [5].

In the case of the red–ox mechanism, CO adsorbs on the metal and reacts at the metal–support interface with oxygen from the support surface, forming CO_2 and decreasing the support surface. The latter is then reoxidized by H_2O, forming H_2. This mechanism was supported by kinetic studies, TPD, TPR and oxygen storage capacity measurements [26,28,33,34].

In our efforts to develop single-stage Pt-based WGS catalysts for fuel cell applications, we found a strong influence of the support on catalyst activity [16]. Here we report on the influence of the oxide support (ZrO_2, CeO_2, or TiO_2) of Pt-based catalysts on the mechanistic reaction sequence(s) for the WGS reaction. We performed kinetic pulse transient studies using CO, H_2O, and N_2O and in situ FTIR spectroscopic measurements to elucidate elementary reaction steps and identify

reaction intermediates during WGS reaction sequence. We used N_2O to reoxidize the oxide surface without regeneration of OH groups to study the role of surface OH groups in the WGS reaction. In this way, we avoid high-temperature dehydroxylation of the catalyst surface, preventing any structural changes (e.g., decreased Pt dispersion) in the catalyst. In Part 2 [16], we report on the use of these concepts to develop an active, selective, and stable single-stage WGS catalyst.

2. Experimental

2.1. Catalyst preparation

The following commercial supports were used: TiO_2 (Degussa, P-25), CeO_2 (Aldrich), and ZrO_2 (Daiichi Kagaku Kogyo, RC100). The catalysts were prepared by wet impregnation of the solid supports with aqueous solutions of H_2PtCl_6 (Aldrich) to yield catalysts with 0.5 wt% Pt. The catalysts were dried at 75 °C for 2 h in vacuum and subsequently calcined at 450 °C for 4 h.

2.2. Characterization

Platinum content of the catalysts was determined using Philips X-ray fluorescence spectrometer (PW 1480). The BET surface area of the supports and catalysts were measured using the BET method on Micromeritics ASAP 2400. Pt dispersions were measured by H_2 chemisorptions at room temperature using a Micromeritics Chemisorb 2750. Teschner et al. [36] showed in a detailed study that hydrogen spillover does not occur significantly on Pt/CeO_2 at lower temperatures (i.e., 20 °C), resulting in reliable dispersion measurements. Therefore, H_2 spillover from Pt particles to the support surface is not influencing dispersion measurements in the case of ceria-supported catalysts. The properties of the supports and the catalysts are summarized in Table 1.

2.3. Pulse experiments

Kinetic transient pulse experiments were performed at 300 °C, at atmospheric pressure using a fixed-bed reactor. A 50-mg catalyst sample was placed between two quartz plugs in a quartz tubular reactor ($d = 4$ mm). For all of the experiments described below, the gases (He, H_2, CO, and N_2O) used were of >99.9% purity. The catalyst was first reduced at 300 °C in 10 vol% H_2/He, 30 mL/min flow for 1 h. After this the catalyst was heated at 330 °C in He (30 mL/min) for 30 min. Pulse experiments were then carried out by contacting fixed amounts of reactant gases with catalyst at 300 °C using He as carrier gas. Each pulse contained 3.9 μmol of respective gas (CO and N_2O). H_2O (1.0 μL) was injected using a microsyringe directly into the reactor. Pulses were repeated until the responses for reactants and products no longer changed. To determine the products formed, the outlet of the reactor was directly connected to a Porapak column (5 m, 100 °C) and a thermal conductivity detector (TCD). Downstream to the TCD detector, gases were analyzed by an online mass spectrometer (Balzers QMS 200 F). Quantitative determination of all gaseous products, except of H_2 and H_2O, was obtained from TCD data with accuracy not below ±0.1 μmol/g_{cat}. H_2 was detected by MS; the data for H_2 are semiquantitative for each catalyst, and quantitative comparison between catalysts is not applicable.

Table 1
Supports and catalysts properties

Sample	Calcination time, T	XRF Pt (wt%)	Pt dispersion (%) at 25 °C	Surface Pt (μmol/g)	BET (m^2/g)
CeO_2	500 °C, 4 h	–	–	–	85
TiO_2	500 °C, 4 h	–	–	–	50
ZrO_2	500 °C, 4h	–	–	–	25
Pt/CeO_2[a]	450 °C, 4 h	0.54	65	16.6	81
Pt/TiO_2	450 °C, 4 h	0.49	55	14.1	48
Pt/ZrO_2	450 °C, 4 h	0.47	60	15.4	22

[a] H_2 chemisorption at 0 °C gave 61% Pt dispersion.

2.4. FTIR studies

The FTIR spectra were recorded using a Bruker Vector 22 with MCT detector under flow conditions [5% CO/He, 10% H_2O/He, and (5% CO + 10% H_2O)/He] at the same temperature used in the kinetic experiments (300 °C). Pulse experiments were mimicked by fast switching between He and a mixture of He containing CO or H_2O.

3. Results

A typical experimental result during subsequent pulsing of CO and H_2O over a catalyst (e.g., Pt/CeO_2) at 300 °C is presented in Fig. 2. Cumulative consumption and formation of reactants and products, respectively, were quantified; the data are shown in Table 2. We started the pulse sequence experiments with hydroxylated catalyst surfaces.

3.1. Pt/CeO_2

The first CO pulse resulted in partial CO consumption and production of CO_2. In the subsequent CO pulses, the amounts of CO_2 formed decreased. After four CO pulses, only traces of CO_2 were observed, and the amount of CO detected in the outlet of the reactor was close to the amount of CO in the pulse applied (±0.1 μmol/g_{cat}). No H_2 formation was observed. The cumulative amount of CO_2 formed (68 μmol/g, Table 2) was much lower than the amount of CO consumed (158 μmol/g) during pulsing. FTIR spectra of Pt/CeO_2 after exposure to CO at the same temperature (compare Figs. 3 and 4) showed a band at 2050–2060 cm^{-1} typical for linearly adsorbed CO on Pt [37], a band at 2856 cm^{-1} corresponding to the C–H stretching of formate [31], and bands in the spectra interval 1600–1300 cm^{-1} corresponding to carbonate and/or formate on ceria [13,31,37]. These species were relatively stable and could not be removed by flushing with He at 300 °C.

After CO, the subsequent H_2O pulses resulted in simultaneous production of CO_2 and H_2 (Fig. 2, Table 2). Most of the CO_2 and H_2 was formed during the first two pulses. The

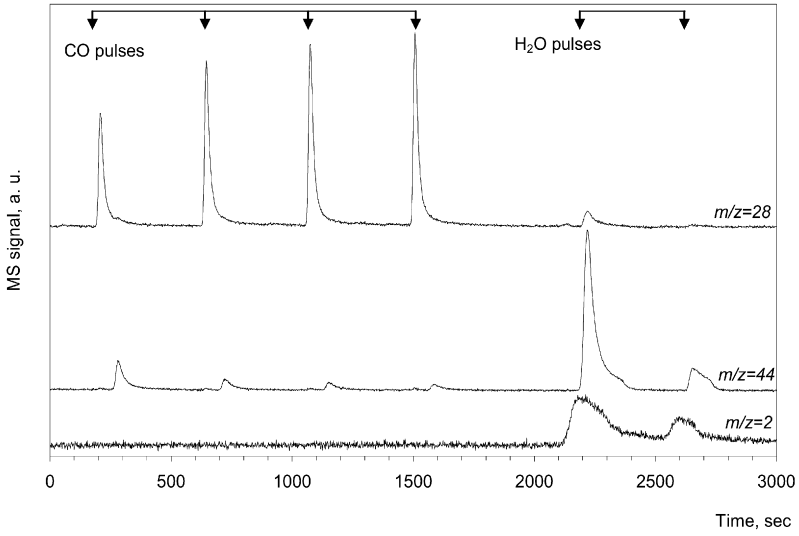

Fig. 2. Typical MS response for pulse experiment over Pt/CeO_2 catalyst reduced at 300 °C in H_2(10%)/He flow. Four pulses CO are followed with two pulses H_2O. Difference in time between products detected is due to their separation with GC (Porapak column).

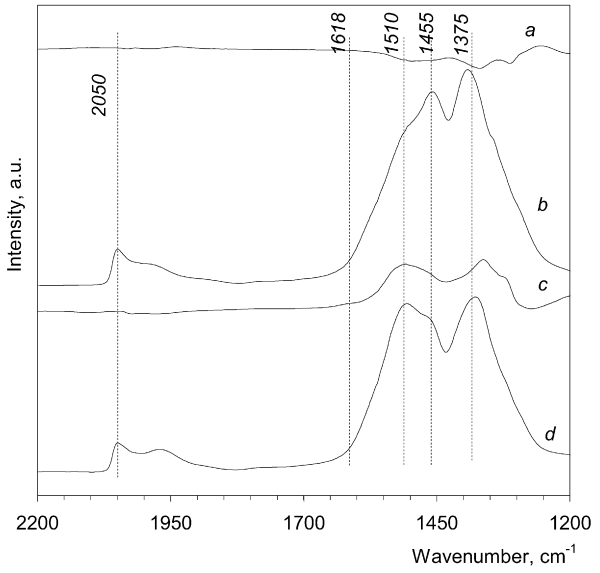

Fig. 3. FTIR spectra at 300 °C of Pt/CeO_2 catalyst; reduced in 10 vol% H_2/He flow (a); after CO pulses (b); after H_2O pulses (c); in situ WGS conditions (d).

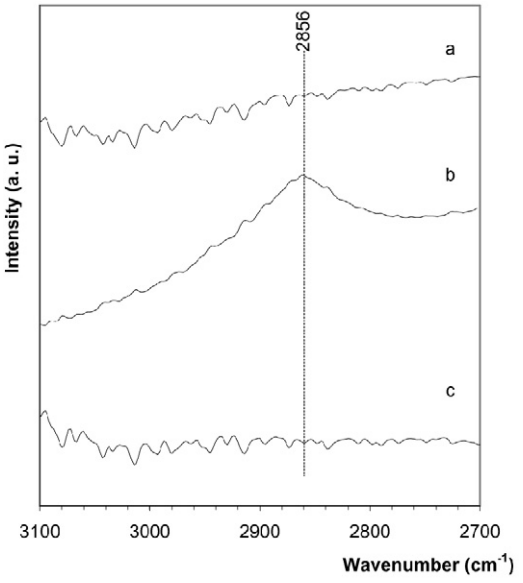

Fig. 4. FTIR spectra at 300 °C of Pt/CeO_2 catalyst; reduced in 10 vol% H_2/He flow (a); after CO pulses (b); after H_2O pulses (c).

Table 2
Analysis of gaseous products during pulse experiments over Pt based catalysts

	Catalyst	(I) CO pulse				(II) H_2O pulse after CO		(III) CO pulse after CO–H_2O			
		CO consumed (μmol/g)	CO_2 released (μmol/g)	C uptake (μmol/g)	H_2 production	CO_2 released (μmol/g)	H_2 production	CO consumed (μmol/g)	CO_2 released (μmol/g)	C uptake (μmol/g)	H_2 production
I	Pt/CeO_2	158	68	90	–	60	+	118	57	60	–
II	Pt/TiO_2	52	51	1	+	0.6	+	49	48	1	+
III	Pt/ZrO_2	40	40	0	+	No	–	37	34	3	+

	Catalyst	(IV) N_2O pulse after CO		(V) CO pulse after CO–N_2O				(VI) H_2O pulse after CO–N_2O–CO	
		CO_2 released (μmol/g)	H_2 production	CO consumed (μmol/g)	CO_2 released (μmol/g)	C uptake (μmol/g)	H_2 production	CO_2 released (μmol/g)	H_2 production
Ia	Pt/CeO_2	60	+	220	135	85	–	56	–
IIa	Pt/TiO_2	0.6	–	52	50	2	–	0.8	+
IIIa	Pt/ZrO_2	No	–	32	31	1	–	0	–

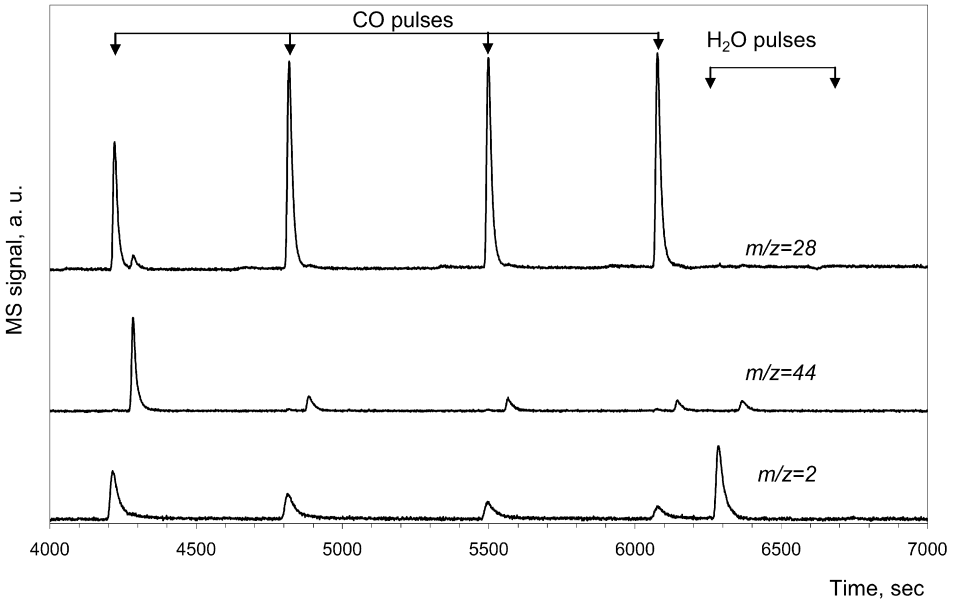

Fig. 5. Typical MS response for pulse experiment over Pt/TiO_2 catalyst reduced at 300 °C in H_2(10%)/He flow. 4 pulses CO are followed with two pulses H_2O. Difference in time between products detected is due to their separation with GC (Porapak column).

next H_2O pulses produced only traces of CO_2 and H_2. Only part of the formate/carbonate groups formed and retained at the surface during CO pulses were reactive to H_2O. After contacting with H_2O, the FTIR band at 2856 cm^{-1}, which corresponded to formate (Fig. 4), disappeared, and the intensity of the bands at 1600–1300 cm^{-1} (Fig. 3), corresponding to formate/carbonate, decreased. However, an appreciable amount of oxygenate species remained on the surface. In quantitative terms, only 60 μmol/g CO_2 was released from the surface during H_2O pulses, and 30 μmol/g "C" was retained at the surface. The next CO–H_2O sequence of pulses showed the same product distribution as in the first sequence.

When N_2O was used instead of H_2O to remove oxygenate species from Pt/CeO_2, the following gaseous products were observed: N_2 due to decomposition of N_2O (not shown) and CO_2 and H_2 due to decomposition of surface formate/carbonate formed during CO pulsing. No O_2 was observed. CO pulses after N_2O treatment (Table 2) showed products (CO_2, no H_2) similar to those during CO pulses over Pt/CeO_2, although somewhat more CO was converted to CO_2. At the same time, the amount of carbon retained on the surface was comparable (85 μmol/g). Pulsing with water after the sequence CO–N_2O–CO resulted in the formation of essentially only CO_2. No H_2 was detected by MS.

3.2. Pt/TiO_2

In contrast to Pt/CeO_2, contacting Pt/TiO_2 with CO resulted simultaneously in the formation of CO_2 and H_2 (Fig. 5, Table 2). With repetitive CO pulses, the amount of CO consumed decreased, in line with decreasing H_2 and CO_2 formation. After four pulses, the amount of CO at the reactor outlet was similar to that in the feed, and only traces of CO_2 and H_2 were detected. The cumulative CO consumption over Pt/TiO_2 was 52 μmol/g. This value was in agreement with the amount of CO_2 formed

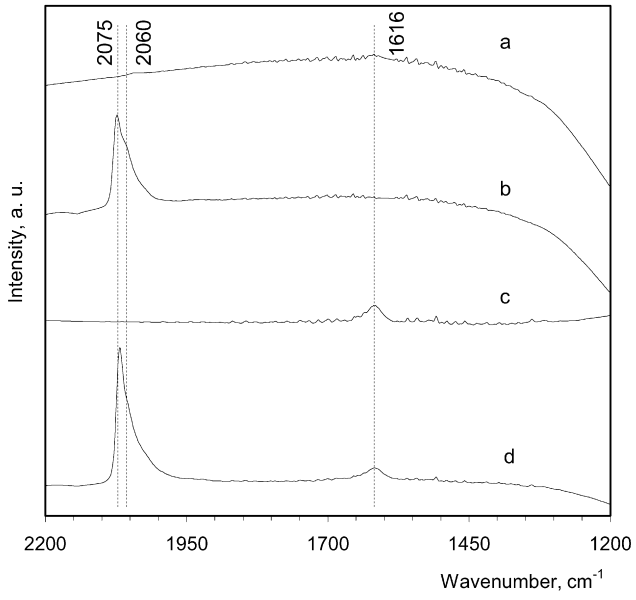

Fig. 6. FTIR spectra at 300 °C of Pt/TiO_2 catalyst; reduced in H_2(10%)/He flow (a); after CO pulses (b); after H_2O pulses (c); in situ WGS conditions (d).

(i.e., 51 μmol/g). Thus, unlike in the case of Pt/CeO_2, no oxygenate species were retained on the Pt/TiO_2 surface. FTIR data (Fig. 6) also showed no formation of carbonate/formate surface species during the CO pulsing. Only CO adsorbed on Pt (Fig. 6) was detectable in the FTIR spectra (2060–2080 cm^{-1}) [9,11] after flushing with He at 300 °C.

The H_2O pulses after CO treatment resulted in H_2 as the main product (Fig. 5); CO_2 was observed in only negligible amounts (0.6 μmol/g). Subsequent CO pulses produced the same gaseous products (CO_2 and H_2) as in the case of the first CO pulse sequence, demonstrating that the surface was regenerated by H_2O and the catalytic cycle was completed. The amount

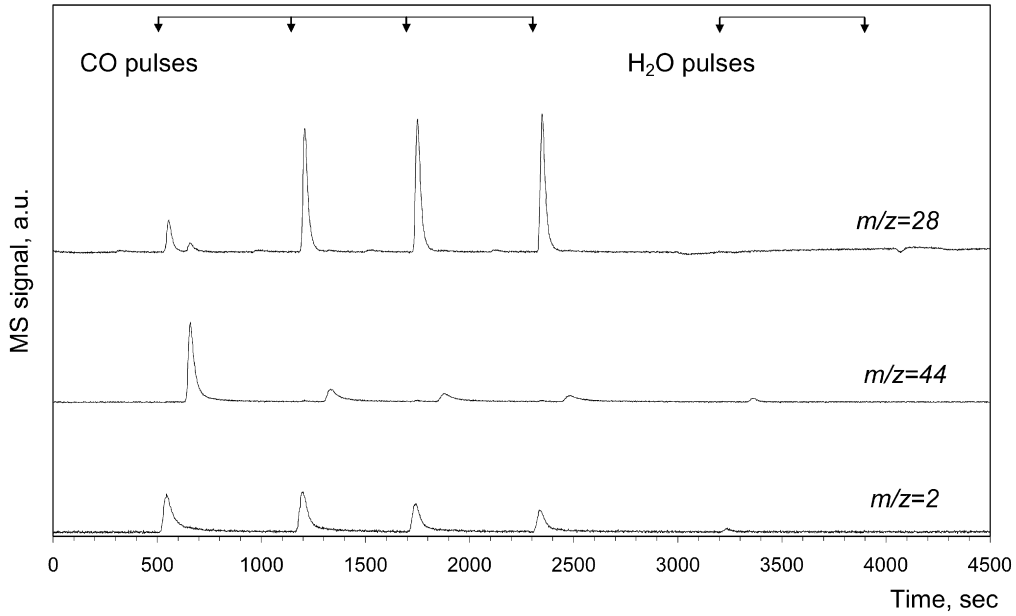

Fig. 7. Typical MS response for pulse experiment over Pt/ZrO_2 catalyst reduced at 300 °C in H_2(10%)/He flow. Four pulses CO are followed with two pulses H_2O. Difference in time between products detected due to their separation with GC (Porapak column).

of CO_2 formed during CO pulses over surface treated with H_2O was 48 μmol/g (Table 2).

When the Pt/TiO_2 was exposed to N_2O pulses after subjecting it to CO pulses (Table 2), no H_2 was observed. N_2 was observed, but no O_2 could be detected, indicating oxygen uptake by the support. The amount of N_2 (not shown) was close to the amount of CO_2 formed during the subsequent CO pulses (52 μmol/g). Subsequent CO pulses (after N_2O) resulted in CO_2 production (50 μmol/g); no H_2 was detected. In case of the CO–N_2O–CO–H_2O sequence, the last H_2O pulse produced the same amount of H_2 (semiquantitatively) as was produced during the H_2O pulse after direct CO exposure.

3.3. Pt/ZrO_2

For the Pt/ZrO_2 catalyst (Fig. 7), the trend was similar to that observed in the case of Pt/TiO_2. CO pulses resulted in release of H_2 and CO_2. The amount of CO consumed was in agreement with the amount of CO_2 released (40 μmol/g), closing the carbon balance. In agreement with this, no formation of stable carbonate/formate group was observed from FTIR (Fig. 8) for Pt/ZrO_2 after CO pulses. Only the band at around 2050–2080 cm^{-1}, related to CO adsorbed on Pt [7], was present.

Surprisingly, in the case of Pt/ZrO_2, H_2O pulses after CO exposure (Table 2) did not produce any gaseous products. However, pulsing H_2O seemed to have regenerated the catalyst, because the subsequent CO pulses resulted in the formation of CO_2 and H_2, similar to the initial CO pulses. In contrast, treatment with N_2O reactivated Pt/ZrO_2 only partially. During the subsequent CO pulses, consumption of CO and production of only CO_2 was observed, and only traces of H_2 were detected.

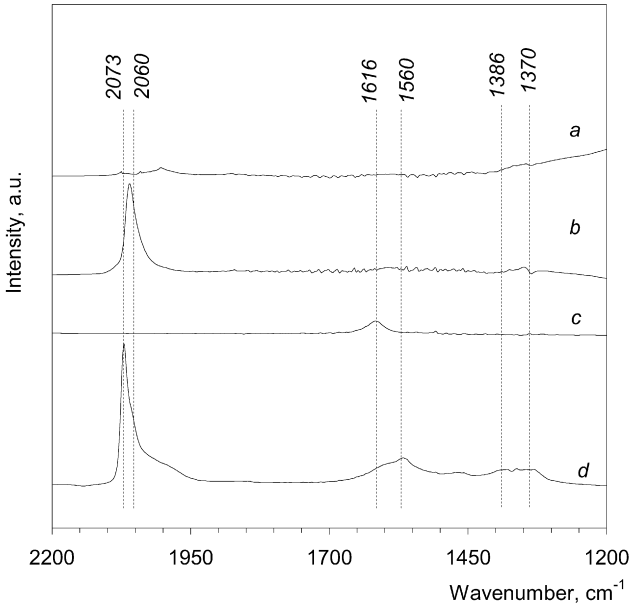

Fig. 8. FTIR spectra at 300 °C of Pt/ZrO_2 catalyst; reduced in H_2(10%)/He flow (a); after CO pulses (b); after H_2O pulses (c); in situ WGS condition (d).

4. Discussion

Kinetic pulse studies were used to follow the elementary steps occurring during the WGS reaction. The results of pulse transient experiments are not directly equivalent to data obtained from steady-state experiments; nonetheless, pulse experiments allow us to rule out those reaction pathways that cannot be induced by sequentially pulsing CO and H_2O. Furthermore, the conclusions obviously hold only for the conditions chosen in this study, because it has been reported elsewhere [38,39] that

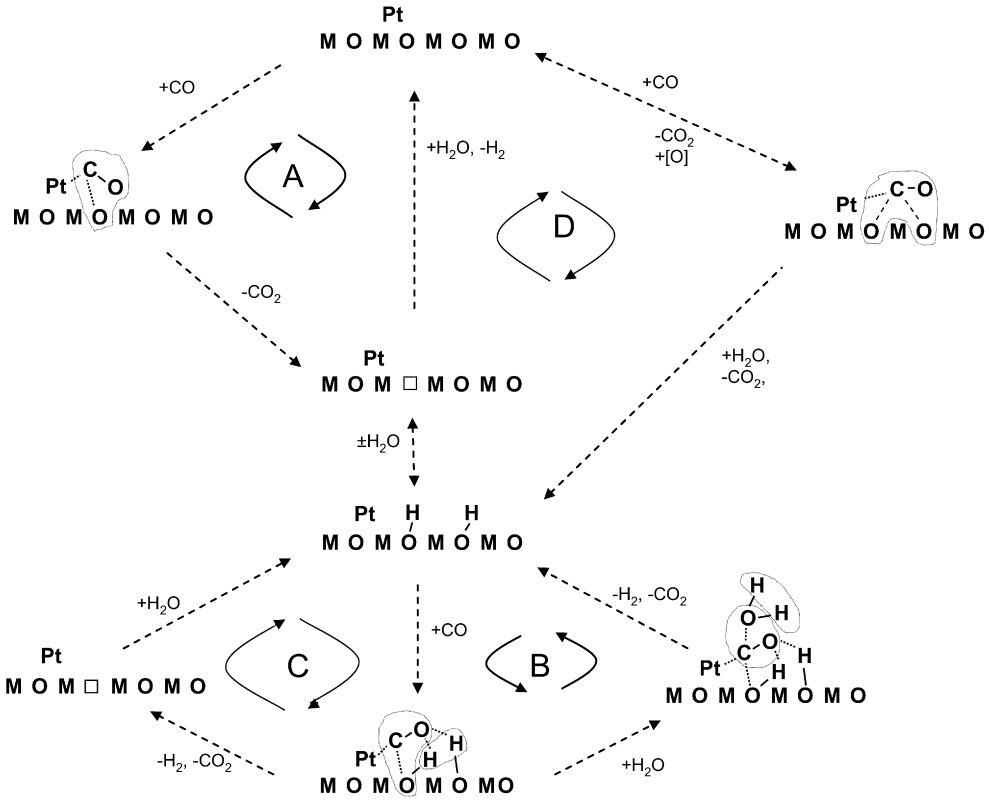

Fig. 9. Role of oxide support on the reaction pathways for WGS. In all cases CO is adsorbed on Pt and reacts at Pt–support interface: A—classical re–dox route; B—associative route; C—associative mechanism with oxide regeneration via re–dox; and D—formation, regeneration of carbonate on oxide.

the dominant reaction mechanism depends on the experimental parameters, such as reaction temperature and gas composition.

As outlined in the Introduction, two mechanistic routes have been reported for the WGS reaction sequence over Pt/CeO_2 catalysts: an associative formate mechanism and a regenerative red–ox mechanism. In our view, there are other possible routes to the WGS reaction over oxide-supported Pt catalysts. Four possible sequences are outlined in Fig. 9: (A) the red–ox route, (B) the associative formate route, (C) the associative formate route with red–ox regeneration of the oxide support, and (D) the carbonate route. In all four sequences, we propose (in agreement with the literature [24–30]) that CO is adsorbed on Pt and reacts at the Pt–support periphery as in a typical bifunctional catalyst. The support oxide plays a role in the activation of water and closure of the WGS catalytic cycle.

The feasible reaction route(s) for each support can be elucidated from kinetic pulse experiments based on the gaseous products formed during sequential CO and H_2O pulses (Table 3). Thus, in the red–ox mechanism, formation of only CO_2 or H_2 should be observed during CO and H_2O pulses, respectively. For the associative formate route, CO pulsing should result not in any gaseous products, but rather in stable intermediates (i.e. surface formate groups [5,6,31,32]), which are decomposed during H_2O pulsing, simultaneously producing CO_2 and H_2. The associative formate route with red–ox regeneration as proposed in Fig. 9 implies that intermediate formate species are not stable and decompose immediately, producing both CO_2 and H_2 during CO pulsing. The subsequent H_2O pulse should only regenerate hydroxyl-groups at the support surface without releasing any gaseous products. In this case (route C), CO_2 is formed, taking oxygen from the oxide support surface, whereas in the classical associative formate mechanism (route B), oxygen for CO_2 is supplied by H_2O.

Table 3
Gaseous products expected during sequential CO and H_2O pulses for each reaction pathway proposed in Fig. 9

Reaction pathway	Expected gaseous products	
	CO pulse	H_2O pulse
Classical red–ox	CO_2	H_2
Associative formate	None	CO_2, H_2
Associative formate with red–ox regeneration	CO_2, H_2	None
Carbonate	None	CO_2

We now discuss the results obtained with Pt catalysts over different supports in view of the various proposed routes. In the case of Pt/CeO_2, the results indicate that the WGS reaction follows an associative formate mechanism, in agreement with earlier reported data [4–6,13,31,32]. Evidence for this comes from the observation in FTIR spectra (Figs. 3 and 4) of formates on Pt/CeO_2 after pulsing CO. This is further supported by the simultaneous formation of H_2 and CO_2 during H_2O pulses (Table 2, row I). Furthermore, the carbon uptake (90 μmol/g) was much higher than would be expected from exclusively CO adsorption on Pt (16 μmol/g if the ratio of CO to surface Pt is 1:1, which is typical for CO adsorption over Pt at room temperature [40]). Because pulsing was done at 300 °C, we should have

expected a much lower CO coverage of Pt, because it is well known that CO desorption from Pt commences at 200 °C [11]. Therefore, most of the C uptake must be related to the formation of formate/carbonate surface species, in agreement with FTIR observations (Figs. 3 and 4). The amount of carbon remaining on the ceria surface (90 μmol/g) was much smaller than the calculated monolayer capacity (6×10^{18} molecules/m^2 [41]) for the CeO_2 support for carbonate and/or formate groups (i.e., 810 μmol/g). It is very difficult to assign the bands observed in Fig. 3 to either formate or carbonate; despite the many significant attempts reported in the literature [5,14,31,37], the bands are very broad and too strongly overlapping to allow definite assignments. However, the band at 2856 cm^{-1} (C–H stretching of formate [31]) shows the presence of formate species on the ceria surface during CO pulses. In this paper, we do not go into the details of differentiating between formate and carbonate bands in the IR spectra (Fig. 3); for the moment, we can only conclude that both oxygenate species were formed during CO pulsing, they were stable, and their formation can be described by the following equations:

$$\text{Pt–CO} + \text{OH}_{(s)} \rightarrow (\text{COOH})_{(s)} \quad (1)$$

and

$$\text{Pt–CO} + 2\text{O}_{(s)} \rightarrow (\text{CO}_3)_{(s)}, \quad (2)$$

where (s) denotes the support site. We conclude that formation of CO_2 and H_2 during the subsequent H_2O pulse was due to the decomposition of formate,

$$(\text{COOH})_{(s)} + \text{H}_2\text{O}_{(g)} \rightarrow \text{CO}_{2(g)} + \text{H}_{2(g)} + \text{OH}_{(s)}, \quad (3)$$

because formate is known to be unstable on ceria in the presence of H_2O [5,31,42]. This is also substantiated by the disappearance of the formate band at 2856 cm^{-1} in the FTIR results (Fig. 4).

In agreement with the literature [43], carbonates were retained on ceria at this temperature even in the presence of water. However, we do not at this point exclude decomposition of part of the surface carbonates during H_2O pulsing,

$$(\text{CO}_3)_{(s)} + \text{H}_2\text{O}_{(g)} \rightarrow \text{CO}_{2(g)} + 2\text{OH}_{(s)}. \quad (4)$$

Both reactions (3) and (4) result in rehydroxylation of the ceria surface, closing the catalytic cycle for the WGS reaction.

In the absence of OH groups, the formate route is not possible. The importance of $OH_{(s)}$ groups in the WGS reaction is confirmed by the experiments with N_2O over Pt/CeO_2-containing formate/carbonate groups (Table 2, row Ia). It is important to emphasize that N_2O is not involved in the WGS reaction. However, the aim of using N_2O here is to decompose the surface formate formed during CO pulses without regenerating the hydroxyl groups. In this way, the catalyst will be free of reactive OH groups, making it possible to probe whether a red–ox pathway (Fig. 9, route A) is involved in the reaction mechanism. During N_2O pulses, both H_2 and CO_2 were formed (Table 2, row Ia), indicating the decomposition of surface formate,

$$(\text{COOH})_{(s)} + \text{N}_2\text{O}_{(g)} \rightarrow \text{CO}_{2(g)} + (1/2)\text{H}_{2(g)} + \text{N}_{2(g)} + \text{O}_{(s)}. \quad (5)$$

The subsequent CO pulse (Table 2, row Ia) did not produce any hydrogen, as expected. Part of the CO was oxidized and released to the gas phase as CO_2. The remaining CO (85 μmol/g) was retained on ceria. The carbon balance was quite good; the amount (85 μmol/g) was remarkably close to the amount of carbon retained (90 μmol/g, as both carbonate and formate in total) in row A after the CO pulse. Because no hydroxyl groups were available (because regeneration was by N_2O, not H_2O), creation of the formate species on the ceria surface could be ruled out. Only carbonates were present. Thus, in the absence of formates, some sites were occupied by carbonates, implying that under WGS conditions, carbonates and formates were competing for surface sites on ceria.

The fact that only carbonates were present and formates were absent is further highlighted by the absence of hydrogen formation during the subsequent H_2O pulse (row Ia). If formates had been present, then we would have seen hydrogen when pulsing water (row I). Only partial decomposition of the carbonates (∼65%) to CO_2 was observed (Table 2, row Ia). This observation unambiguously proves that an associative formate mechanism (reaction (1), route B in Fig. 9) was contributing significantly to H_2 formation. Alternatively, formation of CO_2 during CO pulses also can result from the reduction of the ceria surface according to the sequence

$$\text{Pt–CO} + \text{O}_{(s)} \rightarrow \text{CO}_{2(g)} + *_{(s)} + \text{Pt}, \quad (6)$$

where $*_{(s)}$ denotes an oxygen vacancy on the support. In principle, oxidation of these sites by H_2O can proceed in two ways:

$$*_{(s)} + \text{H}_2\text{O} \rightarrow \text{O}_{(s)} + \text{H}_{2(g)} \quad (7)$$

and

$$*_{(s)} + \text{O}_{(s)} + \text{H}_2\text{O} \rightarrow 2\text{OH}_{(s)}. \quad (8)$$

Reaction (7), which completes a typical red–ox cycle with reaction (6), can be neglected based on the results from the N_2O–CO–H_2O pulse sequence (row Ia), because no H_2 was observed, as would be expected. Formation of hydroxyl groups via reaction (8) is possible.

There is only a subtle difference between reactions (3) and (8). In reaction (3), the oxygen of the OH group comes from the water molecule, and oxygen from ceria is not involved. This is a classical associative mechanism (route B, Fig. 9). In reaction (8), oxygen from ceria is also involved in hydroxyl formation and thus also in formate formation, making this an associative mechanism involving red–ox regeneration (route C, Fig. 9).

Based on the results over Pt/CeO_2 catalyst under these experimental conditions, we conclude that WGS reaction proceeds via an associative mechanism (route B, Fig. 9). We exclude route C from the reaction pathways because no H_2 formation occurred during CO pulses. Route A also is not involved because no H_2 formation occurred during H_2O pulsing after the reduced ceria was oxidized with N_2O (H_2O after CO–N_2O–CO pulses; Table 2, row Ia). At this moment, we do not rule out route D. But because cerium carbonate is stable up to 430 °C [43] and Pt/CeO_2 deactivates due to the blocking of the active sites by carbonate [16], we propose that route D does not contribute to the WGS reaction. This is substantiated by the fact

that no hydrogen was formed during H_2O pulses after the sequence CO–N_2O–CO when only carbonates were present.

Gorte and Zhao [28] recently reported that the WGS reaction proceeds via a red–ox mechanism at 450 °C over Pt/CeO_2 catalyst, based on the responses to CO and H_2O pulses at 450 °C. Both CO_2 and H_2 were formed during CO pulsing [28]. This observation was explained by the interaction of CO with hydroxyl H_2, reducing the ceria and forming H_2 and CO_2. As a result of H_2O pulsing, both CO_2 and H_2 were also formed. It has been claimed that H_2 formation was due to the oxidation of reduced ceria and that CO_2 formation results from the decomposition of carbonate. However, the temperature in the work of Gorte et al. was significantly higher (450 °C) than that used in our study (300 °C). Formates and carbonates are not stable at the higher temperatures, inducing a change in the mechanism.

In the case of Pt/TiO_2, the sequence for the WGS reaction differs from that for ceria discussed above. Unlike in Pt/CeO_2, H_2 is also formed simultaneously with CO_2 during CO pulsing (Table 2, row II). There is only one source for hydrogen in the Pt/TiO_2 catalyst during CO pulsing at 300 °C, i.e., surface hydroxyl groups. Thus, the net reaction can be represented as

$$\text{Pt–CO} + \text{OH}_{(s)} \rightarrow \text{CO}_{2(g)} + (1/2)\text{H}_{2(g)} + \text{Pt} + *_{(s)}, \quad (9)$$

which corresponds to an associative mechanism with red–ox regeneration in our scheme (Fig. 9, route C). It is not clear at this moment which type of hydroxyl group on reduced Pt/TiO_2 surface is relevant for WGS reaction. This determination requires additional studies, which are beyond the scope of this article.

The carbon balance indicates that no carbon species remained on the surface (row II). This finding is also confirmed by in situ FTIR measurements (Fig. 6). The fact that no formate/carbonate species were detected under reaction conditions implies that their decomposition to CO_2 and H_2 is facile. We propose, in agreement with Panagiotopoulou et al. [10], that formate-type intermediates are the only oxygenate species relevant to the WGS sequence over the Pt/TiO_2 catalyst; thus, an associative formate mechanism with a red–ox regeneration is operative. We also can confirm that CO is quantitatively converted to gaseous products in the case of TiO_2. This is unlike ceria, where part of the CO is retained as carbonate, occupying sites for formate formation, which cannot yield any hydrogen.

Contacting the catalyst with water after exposure to CO (Table 2, row II) resulted in hydrogen; no CO_2 was observed, because no oxygenate remained on the surface. The formation of hydrogen indicates that reoxidation of the support occurred according to

$$*_{(s)} + \text{H}_2\text{O}_{(g)} \rightarrow \text{O}_{(s)} + \text{H}_{2(g)}. \quad (10)$$

It was reported earlier that the surface of TiO_2 can be reduced by CO [Eq. (11)] and oxidized by H_2O [44],

$$\text{O}_{(s)} + \text{Pt–CO} \rightarrow \text{CO}_{2(g)} + *_{(s)}. \quad (11)$$

The red–ox nature of TiO_2 is also indicated by the formation of hydrogen during the water pulsing after a CO–N_2O–CO sequence. Therefore, we cannot exclude (as in the case of CeO_2 and ZrO_2 [see below]), the red–ox route (route A, Fig. 9) for the WGS reaction in Pt/TiO_2, implying involvement of the sequence of reactions (10) and (11). Quantitative determination of the amount of H_2 produced during CO pulsing (Table 2, row II) would enable discrimination, but unfortunately, these data were not available.

We conclude from the above results that both oxygen vacancies on the reduced TiO_2 and hydroxyl groups on TiO_2 can take part in the catalysis of the WGS reaction. Thus, both the associative route with red–ox regeneration pathway (route C, Fig. 9) and the classical red–ox pathway (Fig. 9, route A) may significantly contribute in the WGS mechanism. Route B can be excluded, because no CO_2 formation occurred during H_2O pulses (Table 2, row II). Route D again can be ruled out because no CO_2 formation occurred during H_2O pulsing after the reduced titania was oxidized with N_2O (H_2O after CO–N_2O–CO pulses; Table 2, row IIa), and because carbonate was not present on TiO_2 after CO pulsing, according to FTIR data (Fig. 6). The activity of Pt/TiO_2 seems to be determined by the ability of TiO_2 to undergo red–ox as well as to allow formation of OH groups. Decomposition of the intermediate formate species seems facile.

For the Pt/ZrO_2 catalyst, the WGS reaction seemed to follow an associative route with red–ox regeneration (Fig. 9, route C). During CO pulsing, the catalyst showed behavior similar to that of Pt/TiO_2. CO pulsing results in CO_2 and H_2 formation, which can be described by reaction (9), were part of route C in Fig. 9. The carbon balance indicates that no carbon species remained on the surface (Table 2, row III). This is also confirmed by in situ FTIR measurements (Fig. 8). It is still not clear whether intermediate formate species were involved. They could be observed with in situ FTIR during reaction (Fig. 8), but as soon as the flow was switched to inert gas, the bands disappeared from the spectrum. During H_2O pulsing, no gaseous products were observed, but the catalyst was able to produce CO_2 and H_2 at the next CO pulse. From these findings, we conclude that route B was not operative and that catalyst activation occurred mainly due to hydroxyl groups formed according to reaction (8).

Normally, ZrO_2 is considered a nonreducible oxide, even though evidence exists that the surface is partly reducible at relatively higher temperatures (>600 °C) [45]. However, the fact that at 300 °C, CO_2 and H_2 were formed on a hydroxylated surface (Table 2, row III) implies that the surface OH groups were converted, leaving an oxygen vacancy (Fig. 9, route C). When this surface was reoxidized by N_2O, no active hydroxyls were formed. The observation that CO_2 was detected (Table 2, row IIIa) during CO pulsing after the CO–N_2O sequence indicates that some lattice oxygen could be removed even at 300 °C (6). Therefore, both observations demonstrate that ZrO_2 was able to provide oxygen. We speculate that low-coordination sites in the zirconia surface were responsible. Accordingly, regeneration occurred according to reaction (8), similar to the situation for titania. The gaseous product distribution during pulse experiments indicates that the WGS reaction over Pt/ZrO_2 followed the associative mechanism with red–ox regeneration (Fig. 9, route C). Routes A, B, and D can be excluded, because there were no gaseous products during H_2O pulsing (Table 2, row III). Recently, Trovarelli et al. [46], using isotopic transient kinetics (^{12}CO and ^{13}CO) and in situ DRIFTS at 200 °C, con-

cluded that oxygenates, not excluding formate, are involved as a reaction intermediate, in agreement with our conclusion.

5. Conclusions

The reducibility of the support, as well as the stability of formate and carbonate species together, determine the reaction pathways contributing to the WGS reaction. Water activation is achieved over the support through formation of surface hydroxyl groups on oxides and/or oxidation of the reduced support with H_2O, resulting in H_2 formation. Under the experimental conditions of this work (300 °C), it appears that the classical associative mechanism (route B) is operating for Pt/CeO_2. In Pt/ZrO_2, the dominant reaction pathway is the associative formate route with red–ox regeneration (route C), implying that OH groups react with CO, leaving oxygen vacancies. This result is surprising, because reduction of ZrO_2 is much more difficult than reduction of CeO_2. Apparently, the remarkable stability of surface formates on CeO_2 contributes to this. Finally, for Pt/TiO_2, both the associative formate route with red–ox regeneration (route C) and the classical red–ox route (route A) are possible reaction pathways contributing to the WGS reaction. Pt/TiO_2 was the only catalyst able to dissociate H_2O to H_2 while reoxidizing oxygen vacancies generated by reduction with CO.

Acknowledgments

The authors thank Ing. L. Vrielink for the XRF and BET analysis and Ing. B. Geerdink and K. Altena-Schildkamp for technical assistance. Financial support was provided by the STW (project 790.36.030, The Netherlands).

References

[1] D.S. Newsome, Catal. Rev. Sci. Eng. 21 (1980) 275.
[2] C.H. Bartolomew, R.J. Farrauto, in: C.H. Bartolomew, R.J. Farrauto (Eds.), Fundamentals of Industrial Catalytic Processes, Wiley, Hoboken, NJ, 2006, p. 909.
[3] W. Ruettinger, O. Ilinich, R.J. Farrauto, J. Power Sources 118 (2003) 61.
[4] G. Jacobs, S. Ricote, B.H. Davis, Appl. Catal. A 302 (2006) 14.
[5] G. Jacobs, U.M. Graham, E. Chenu, P.M. Patterson, A. Dozier, B.H. Davis, J. Catal. 229 (2005) 499.
[6] A. Goguet, S.O. Shekhtman, R. Burch, C. Hardcare, F.C. Meunier, G.S. Yablonsky, J. Catal. 237 (2006) 102.
[7] E. Chenu, G. Jacobs, A.C. Crawford, R.A. Keogh, P.M. Patterson, D.E. Sparks, B.H. Davis, Appl. Catal. B 59 (2005) 45.
[8] E. Xue, M. O'Keeffe, J.R.H. Ross, Surf. Sci. Catal. 130 (2000) 3813.
[9] Y. Sato, K. Terada, S. Hasegawa, T. Miyao, S. Naito, Appl. Catal. A 296 (2005) 80.
[10] P. Panagiotopoulou, A. Christodoulakis, D.I. Kondarides, S. Boghosian, J. Catal. 240 (2006) 114.
[11] H. Iida, A. Igarashi, Appl. Catal. A 298 (2006) 152.
[12] P.S. Querino, J.R.C. Bispo, M.C. Rangel, Catal. Today 107–108 (2005) 920.
[13] S.Y. Choung, M. Ferrandon, T. Krause, Catal. Today 99 (2005) 257.
[14] S. Ricote, G. Jacobs, M. Milling, Y. Ji, P.M. Patterson, B.H. Davis, Appl. Catal. A 303 (2006) 35.
[15] W. Ruettinger, X. Liu, R.J. Farrauto, Appl. Catal. B 65 (2006) 135.
[16] K.G. Azzam, I.V. Babich, K. Seshan, L. Lefferts, part 2, J. Catal. (2007), in press.
[17] H. Iida, K. Kondo, A. Igarashi, Catal. Commun. 7 (2006) 240.
[18] O. Goerke, P. Pfeifer, K. Schubert, Appl. Catal. A 263 (2004) 11.
[19] Brunetti, G. Barbieri, E. Drioli, K.-H. Lee, B. Sea, D.-W. Lee, Chem. Eng. Proc. 46 (2007) 119.
[20] M.E. Adrover, E. Lopez, D.O. Borio, M.N. Pedernera, in: F.N. Noronha, M. Schmal, E.F. Sousa-Aguiar (Eds.), Studies in Surface Science and Catalysis, vol. 167, Elsevier, Amsterdam, 2007, p. 183.
[21] Ch. Han, D.P. Harrison, Chem. Eng. Sci. 49 (1994) 5875.
[22] D. Tibiletti, E.A. Bart de Graaf, S.Ph. Teh, G. Rothenberg, D. Farrusseng, C. Mirodatos, J. Catal. 225 (2004) 489.
[23] O. Pozdnyakova, D. Teschner, A. Wootsch, J. Kröhnert, B. Steinhauer, H. Sauer, L. Toth, F.C. Jentoft, A. Knop-Gericke, Z. Paál, R. Schlögl, J. Catal. 237 (2006) 17.
[24] M.A. Henderson, Surf. Sci. Rep. 46 (2002) 1.
[25] J.R. Rostrup-Nielsen, in: J.R. Anderson, M. Boudart (Eds.), Catalysis, Science and Technology, vol. 5, Springer-Verlag, Berlin, 1984, p. 1.
[26] K. Takanabe, K. Aika, K. Seshan, L. Lefferts, J. Catal. 227 (2004) 101.
[27] T. Bunluesin, R.J. Gorte, G.W. Graham, Appl. Catal. B 15 (1998) 107.
[28] R.J. Gorte, S. Zhao, Catal. Today 104 (2005) 18.
[29] P. Panagiotopoulou, D.I. Kondarides, Catal. Today 112 (2006) 49.
[30] D.C. Grenoble, M.M. Estadt, D.F. Ollis, J. Catal. 67 (1981) 90.
[31] G. Jacobs, E. Chenu, P.M. Patterson, L. Williams, D. Sparks, G. Thomas, B.H. Davis, Appl. Catal. A 258 (2004) 203.
[32] G. Jacobs, S. Ricote, U.M. Grahm, P.M. Patterson, B.H. Davis, Catal. Today 106 (2005) 259.
[33] S. Hilaire, X. Wang, T. Luo, R.J. Gorte, J. Wagner, Appl. Catal. A 215 (2001) 271.
[34] X. Wang, R.J. Gorte, Appl. Catal. A 247 (2003) 157.
[35] H. Sakurai, T. Akita, S. Tsubota, M. Kiuchi, M. Haruta, Appl. Catal. A 291 (2005) 179.
[36] D. Teschner, A. Wootsch, T. Roder, K. Matusek, Z. Paal, Solid State Ionics 141–142 (2001) 709.
[37] Holmgren, B. Andersson, D. Duprez, Appl. Catal. B 22 (1999) 215.
[38] D. Tibiletti, A. Goguet, F.C. Meunier, J.P. Breen, R. Burch, Chem. Commun. 14 (2004) 1636.
[39] A. Goguet, F.C. Meunier, D. Tibiletti, J.P. Breen, R. Burch, J. Phys. Chem. B 108 (2004) 20240.
[40] P.B. Wells, Appl. Catal. 18 (1985) 259.
[41] S. Sharma, S. Hilaire, J.M. Vohs, R.J. Gorte, H.W. Jen, J. Catal. 190 (2000) 199.
[42] G. Jacobs, P.M. Patterson, L. Williams, D. Sparks, B.H. Davis, Catal. Lett. 96 (2004) 97.
[43] X. Liu, W. Ruettinger, X. Xu, R. Farrauto, Appl. Catal. B 56 (2005) 69.
[44] M. Calatayud, A. Markovits, M. Menetrey, B. Mguig, C. Minot, Catal. Today 85 (2003) 125.
[45] J. Zhu, S. Albertsma, J.G. van Ommen, L. Lefferts, J. Phys. Chem. B 109 (2005) 9550.
[46] D. Tibiletti, F.C. Meunier, A. Goguet, D. Reid, R. Burch, M. Boaro, M. Vicario, A. Trovarelli, J. Catal. 244 (2006) 183.